Journal of Zhejiang University-SCIENCE A (Applied Physics & Engineering)
ISSN 1673-565X (Print); ISSN 1862-1775 (Online)
www.jzus.zju.edu.cn; www.springerlink.com
E-mail: jzus@zju.edu.cn

# Development and validation of a model for predicting wheel wear in high-speed trains*

Gong-quan TAO[1], Xing DU[1], He-ji ZHANG[1], Ze-feng WEN[†‡1], Xue-song JIN[1], Da-bin CUI[2]

(*[1]State Key Laboratory of Traction Power, Southwest Jiaotong University, Chengdu 610031, China*)

(*[2]Department of Mechanical Engineering, Emei Campus of Southwest Jiaotong University, Emei 614202, China*)

[†]E-mail: zfwen@home.swjtu.edu.cn

Received Oct. 21, 2016; Revision accepted June 5, 2017; Crosschecked July 12, 2017

**Abstract:** In this paper, we present a comprehensive model for the prediction of the evolution of high-speed train wheel profiles due to wear. The model consists of four modules: a multi-body model implemented with the commercial multi-body software SIMPACK to evaluate the dynamic response of the vehicle and track; a local contact model based on Hertzian theory and a novel method, named FaStrip (Sichani *et al*., 2016), to calculate the normal and tangential forces, respectively; a wear model proposed by the University of Sheffield (known as the USFD wear function) to estimate the amount of material removed and its distribution along the wheel profile; and a smoothing and updating strategy. A simulation of the wheel wear of the high-speed train CRH3 in service on the Wuhan-Guangzhou railway line was performed. A virtual railway line based on the statistics of the line was used to represent the entire real track. The model was validated using the wheel wear data of the CRH3 operating on the Wuhan-Guangzhou line, monitored by the authors' research group. The results of the predictions and measurements were in good agreement.

**Key words:** High-speed train; Wheel profile; Wheel/Rail contact; Wheel wear prediction
http://dx.doi.org/10.1631/jzus.A1600693 **CLC number:** TH161.12

## 1 Introduction

Wear at the wheel/rail interface plays a key role in determining the reliability of railway transportation, and has a deep effect on vehicle dynamics and running stability, especially for high-speed trains. The equivalent conicity, widely used by vehicle and infrastructure departments to evaluate the dynamic performance of vehicles, increases gradually with the evolution of the profile shape due to wear. High conicity may lead to transient instability of bogies at some specific locations, possibly triggering an instability alarm (Wang J.B. *et al*., 2016). To ensure running stability and comfort, particularly from the viewpoint of safety, worn wheels have to be periodically re-profiled. In the past, China lacked operational experience with high-speed trains. Long-term tracking tests were performed to obtain the evolution characteristics of wheel wear and their effects on vehicle dynamic behavior. Maintenance strategies and interventions were designed based on these long-term tracking tests. Even if wheel wear data collected by field measurement is reliable, its collection is very time-consuming and increases economic costs. Usually, the collection of the data requires at least several months or even years. Therefore, there is an urgent need to develop a reliable wheel wear model to predict the evolution of wheel profiles due to wear. Due to the large geographical span of ballastless

‡ Corresponding author
* Project supported by the National Natural Science Foundation of China (Nos. U1434201, 51275427, and 51605394), and the Scientific Research Foundation of State Key Laboratory of Traction Power (No. 2015TPL_T01), China
ORCID: Gong-quan TAO, http://orcid.org/0000-0002-1836-2363

track lines and complex climatic conditions, the operating environments of high-speed trains in China are very complicated. The length of the longest high-speed railway line, the Beijing-Guangzhou line, is about 2300 km. A high-speed train runs on this line from dry areas in the north to damp areas in the south. These factors make it very difficult to predict the wheel wear of high-speed trains.

Wear prediction models are very complex mathematical tools. Their development requires the integration of several tasks, such as vehicle-track dynamic simulation, wheel/rail local contact solutions, local wear estimation, and numerical methods. Wheel wear prediction is a popular topic in railway research. Jendel (2002) proposed a wear prediction tool to calculate the wheel wear of vehicles operating on the commuter rail network in Stockholm. The tool consists of a vehicle model, railway network definition, and Archard (1953)'s wear model with associated wear maps. The vehicle dynamic model is implemented in GENSYS MBS software. The contact between the wheel and rail is solved by Hertzian theory and Kalker (1982)'s simplified theory (FASTSIM algorithm) in the normal and tangential directions, respectively. However, the elastic contribution to the creep is neglected. The simulated wheel profiles coincide well with measured profiles in terms of flange thickness, flange height, flange inclination, and the area worn away. Enblom and Berg (2005) improved the KTH wear model further by taking into account the influence of the elastic contribution to the sliding velocity. Braghin *et al.* (2006) presented a fast and reliable wear prediction model. The biggest difference between their model and the KTH wear model is the wear function. The wear function (known as the USFD wear function) adopted by Braghin *et al.* (2006) was developed by the University of Sheffield, UK (Lewis and Dwyer-Joyce, 2004; Lewis *et al.*, 2010) and relates the wear rate to a wear index. Li *et al.* (2011) developed a wheel profile wear prediction method that combines the dynamics of the railway vehicle and track, Kalker (1990)'s complete rolling contact theory, and Archard (1953)'s wear model. This model is very complicated and time-consuming. Ding *et al.* (2014) proposed a wheel wear model to predict the evolution of the wheel profile shape of a heavy haul freight car. The semi-Hertzian method (Ayasse and Chollet, 2005) and FASTSIM algorithm were used to solve the normal and tangential contact problems, respectively. The wheel wear function proposed by Zobory (1997) was used to evaluate the material removed by wear. Four types of freight car with two load states, empty and heavy, operating in China's Ring-line during the reliability tests were considered in a simulation. The simulated wear spreading was narrower than the measured spreading. Moreover, the wear rates of the simulation were larger than those of the field measurements. Subsequently, a corrected Zobory (1997)'s wear function was presented (Ding *et al.*, 2013). Results indicated that the simulated wear was in good agreement with field data using the improved model. Based on statistical methods, Han and Zhang (2015) proposed a novel wheel wear prediction model to estimate the wheel wear of high-speed trains. This method is more like a mathematical fit of measured worn wheel profiles rather than a wear prediction model. A powerful wear prediction model was developed and validated by the University of Florence (Auciello *et al.*, 2012; Ignesti *et al.*, 2012a; 2012b; 2013; Innocenti *et al.*, 2014). It can be used to evaluate the evolution of both wheel and rail profiles due to wear. However, the focus was mainly on ordinary speed trains.

In this study, we present a comprehensive model which can predict the evolution of high-speed train wheel profiles due to wear. It includes four parts: a multi-body model of the CRH3 high-speed train; a detailed local contact model to re-calculate the contact problem to obtain the local creep and shear stress distribution at the contact patch; a wear model based on the USFD wear function to estimate the amount of material removed and its distribution along the wheel profile; and a smoothing and updating strategy. Due to the complexity of wheel/rail interface environments, as stated previously, it is unlikely that a wear function obtained by laboratory tests could be used directly. Generally, a testing laboratory simulates only one wheel/rail interface environment. Field measured wheel profiles of high-speed trains running on the Wuhan-Guangzhou high-speed railway line were used to modify the original USFD wear function. The validated wear model can be used to optimize wheel profiles from the wear viewpoint and enable the design of more reasonable and economical maintenance plans.

## 2 General architecture of the wheel wear prediction model

The general architecture of the model to predict the evolution of high-speed train wheel profiles due to wear is shown in Fig. 1. It consists of four modules: (1) a multi-body simulation of railway vehicle-track dynamics; (2) a local contact model; (3) wear calculation; and (4) smoothing and updating of the wheel profile.

Some assumptions have been introduced to make the simulation more feasible:

1. The rails are not subjected to wear and the rail profiles maintain their original profile (60 kg/m rail profile used in China) during the whole simulation process. This is based on the fact that the wear evolution of rails is minor compared to that of wheels in Chinese high-speed railway lines.

2. The output of the wheel profile is a mean wheel profile, which is used in the dynamic simulations in the next step.

3. The whole simulation process is divided into a series of discrete steps, in which the wheel profile remains unchanged during the dynamic simulations and is updated after each step.

The wheel wear prediction begins with the vehicle and track dynamic simulation, which is conducted using the commercial software SIMPACK. The global contact parameters, i.e., normal force $P$, global creepages ($\upsilon_x$, $\upsilon_y$), spin $\varphi$, and contact position on wheels cpw and rails cpr, are outputted at each integration step of the vehicle-track dynamic simulation. Those parameters are further used in the local contact analysis to obtain the contact patch dimension (semi-axes $a$ and $b$ of the contact ellipse in the rolling and lateral directions, respectively), normal pressure ($P_{3j}$) with Hertz theory, local tangential stresses ($P_{tj}$), and local creepage ($\gamma_j$) distribution within the contact patch with the novel and versatile method FaStrip. Then the wear function USFD, which associates the energy dissipated in the wheel/rail contact patch with the amount of worn material removed from the contact surface, is used to evaluate the wheel wear. Finally, the wheel profile superimposed with wear is smoothed, and subsequently updated through suitable numerical procedures.

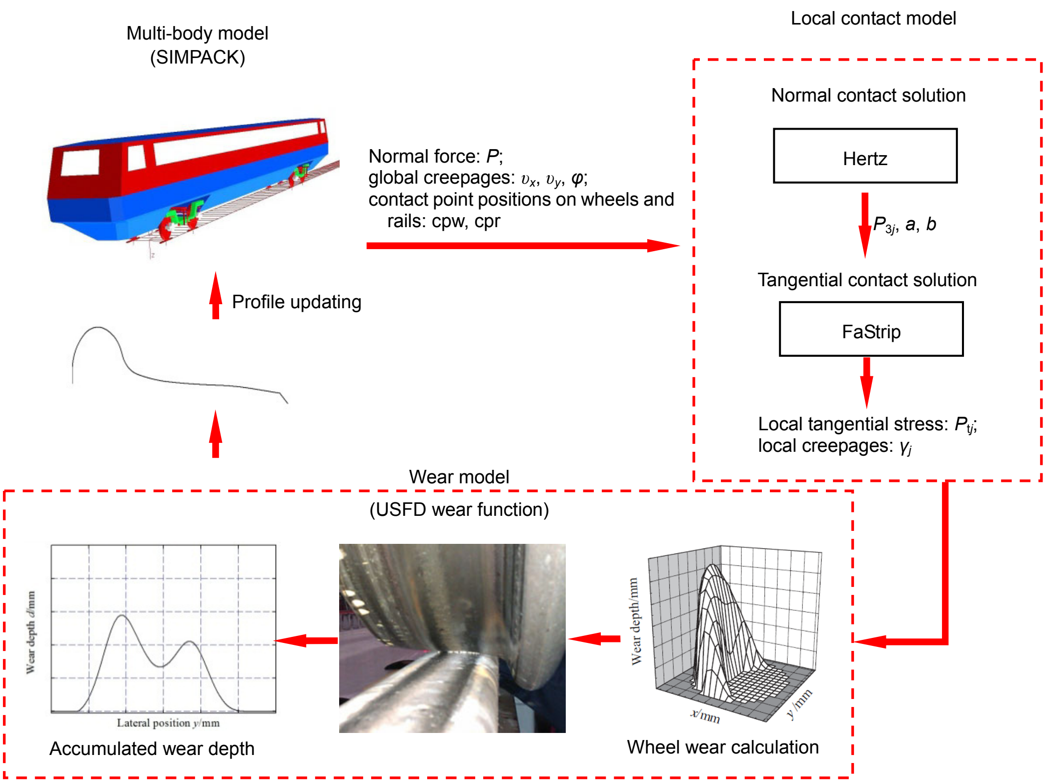


**Fig. 1 General architecture of the wheel wear prediction model**

## 3 Description of the wheel wear prediction model

Here, we describe in detail the four parts of the wheel wear prediction model proposed in this paper.

### 3.1 Multi-body model

The trailed vehicle of the electric multiple unit (EMU) CRH3, which is one of the main high-speed trains running in China, was considered in this study (Fig. 2). The wheel profile type of the CRH3 is called S1002CN (Fig. 3), which originates from type S1002. The flange thickness is 34.5 mm. The wheelset's back-to-back distance is 1353 mm.

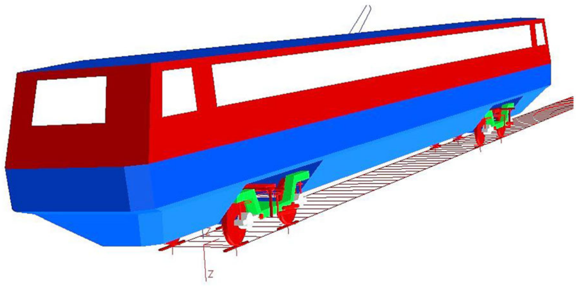

**Fig. 2 Multi-body model of the CRH3**

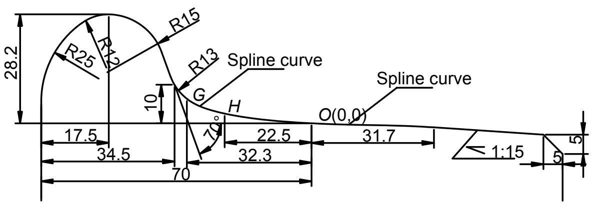


**Fig. 3 S1002CN wheel profile (unit: mm)**

The bogie is the core component of high-speed trains. As in most passenger trains, the bogie has two suspension systems, but the suspension systems of high-speed trains are more complex and versatile to ensure the vehicle's stability and reliability at higher speeds. Fig. 4 illustrates a bogie built in the SIMPACK environment. The primary suspension, which links the axle boxes to the bogie frame comprises a flexi-coil, axle lever bushing, and primary vertical damper (four per bogie). The flexi-coil is made up of two coaxial springs, which mainly provide the vertical stiffness in this system. The longitudinal and lateral stiffness are provided mainly by the axle lever bushing, which is closely related to the vehicle's stability at high-speeds on straight tracks. A nonlinear primary damper is responsible for the damping of the vertical relative displacements.

The secondary suspension system includes the following elements:

(1) Two air springs for the longitudinal, lateral, and vertical stiffness;

(2) Two nonlinear lateral dampers;

(3) Four nonlinear yaw dampers (two on each side of the bogie);

(4) A torsion bar;

(5) A nonlinear traction rod, to transmit the traction and braking force.

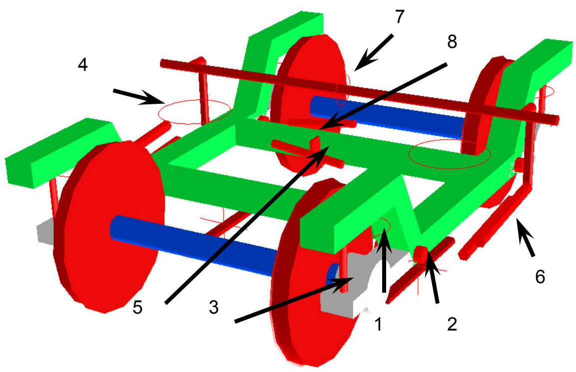


**Fig. 4 Trailer bogie of a CRH3 train built in SIMPACK**
1: flexi-coil spring; 2: axle lever bushing; 3: primary vertical damper; 4: air spring; 5: secondary lateral damper; 6: secondary yaw damper; 7: anti-roll bar; 8: secondary lateral bump stop; 9: traction rod (not visible in the figure)

The multi-body model of the CRH3 trailer vehicle was implemented with the commercial multi-body software SIMPACK. The model includes 15 rigid bodies: one coach, two bogie frames, four wheel-sets, and eight axle boxes. The structural elasticity of all vehicle components is ignored. All the force elements have been modelled as viscoelastic force elements, taking all the mechanical non-linear characteristics into account, such as primary vertical dampers, secondary lateral dampers, yaw dampers, and secondary lateral bump stops. A measured irregularity on a high-speed railway line in China was applied in the dynamic simulation (Fig. 5). The tangential contact solution in the dynamic simulation is based on Kalker (1982)'s simplified theory, implemented in the FASTSIM algorithm. The coefficient of friction is assumed to be a constant value of 0.3.

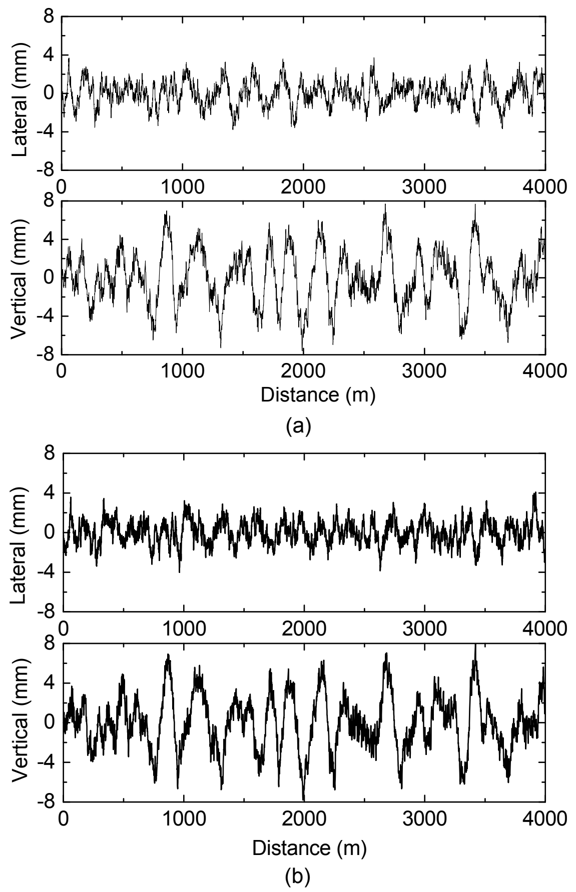


**Fig. 5 Measured irregularity on a high-speed railway line in China: (a) left rail; (b) right rail**

## 3.2 Local contact model

The wheel/rail contact model is the core of wheel and rail damage prediction, such as rolling contact fatigue and wear. A detailed solution of the shear stress distribution in the wheel/rail interface and the division between the regions of stick and slip is required, as well as the local creep within contact patches. Kalker (1982)'s simplified theory, implemented with the FASTSIM algorithm, is the most popular contact model used in multi-body system dynamic simulation and wheel/rail wear prediction to solve the tangential contact problem. The algorithm can estimate reasonable creep forces. However, the shear stress distribution and stick-slip division needed for damage analysis, differ significantly from Kalker (1990)'s complete theory (Sichani *et al.*, 2016). To improve the tangential contact solution, especially for the shear stress distribution and stick-slip division, a novel and versatile method, named FaStrip, was recently proposed by Sichani *et al.* (2016). The novel method combines Kalker (1966)'s strip theory with the simplified theory (Kalker, 1982). The longitudinal and lateral shear stress distributions in the stick area are based on Kalker (1966)'s strip theory:

$$q_x(x,y)=\frac{\mu p_0}{a}\Big[\kappa\sqrt{a^2(y)-x^2} - \kappa'\sqrt{\big(a(y)-d(y)\big)^2-\big(x-d(y)\big)^2}\Big], \tag{1}$$

$$q_y(x,y)=\frac{\mu p_0}{a}\Big[\lambda\sqrt{a^2(y)-x^2} - \lambda'\sqrt{\big(a(y)-d(y)\big)^2-\big(x-d(y)\big)^2}\Big], \tag{2}$$

where $\mu$ is the coefficient of friction, $p_0$ is the maximum Hertzian pressure expressed as $p_0=3N/(2\pi ab)$, $N$ is the normal force, and $a$ and $b$ are the semi-axes in the rolling and lateral directions, respectively. The half-lengths of the patch and the slip area for the strip in the lateral coordinate $y$ are denoted by $a(y)=a\sqrt{1-(y/b)^2}$ and $d(y)$ (Fig. 6), respectively. The terms $\kappa$, $\kappa'$, $\lambda$, and $\lambda'$ as well as $d(y)$ depend on creepages and spin.

$$d(y)=\frac{\sqrt{\eta^2+(1-\psi^2)(\xi-\psi y/a)^2}+\eta\psi}{1-\psi^2}\frac{a}{1-\nu}, \tag{3}$$

$$\kappa=\kappa'=\frac{a(\xi-\psi y/a)}{(1-\nu)d(y)}, \tag{4}$$

$$\lambda=\frac{a\eta}{(1-\nu)d(y)}+\psi, \tag{5}$$

$$\lambda'=\frac{a\eta}{(1-\nu)d(y)}, \tag{6}$$

where $\nu$ is Poisson's ratio. $\xi$, $\eta$, and $\psi$ are non-dimensional creepages ($\upsilon_x$, $\upsilon_y$) and spin ($\varphi$), respectively, defined as follows:

$$\begin{aligned}\xi&=-\frac{G}{2\mu p_0}\upsilon_x,\\ \eta&=-\frac{G}{2\mu p_0}(1-\nu)\upsilon_y,\\ \psi&=-\frac{G}{2\mu p_0}a\varphi,\end{aligned} \tag{7}$$

where $G$ is the equivalent shear modulus.

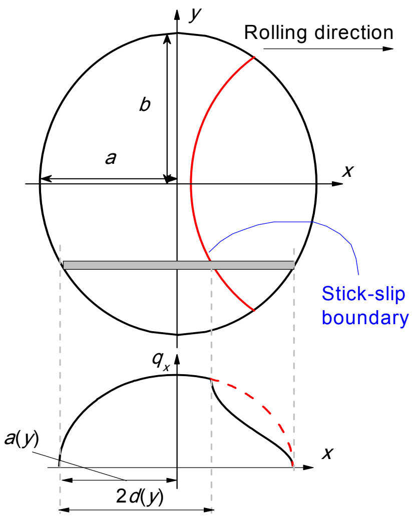


**Fig. 6 Schematic of stick-slip division and shear stress distribution according to the strip theory**

As mentioned by Kalker (1966), the strip theory works well in the case of pure creepage, especially in the case of contact ellipses which are narrow in the rolling direction. However, its accuracy is significantly reduced as the semi-axes ratio of the contact ellipse increases. In addition, spin has a considerable effect on the accuracy of the strip theory, especially for a large spin. To overcome these shortcomings, some improvements need to be made.

The strip formulation should be amended to obtain good accuracy for all types of contact ellipses. Similar to the approach to achieving the flexibility parameters in Kalker (1982)'s simplified theory, the creep forces calculated by strip theory should be equal to those obtained by Kalker (1967)'s linear theory for infinitely small creepages and spin. The creep forces of strip theory can be calculated by integrating Eqs. (1) and (2). Comparing the integrated results with those from Kalker (1967)'s linear theory, three correction factors are defined (Sichani *et al.*, 2016):

$$\begin{cases} c_x = \dfrac{4(1-\nu)}{\pi^2}C_{11}, \\ c_y = \dfrac{4}{\pi^2}C_{22}, \\ c_\varphi = \dfrac{3}{\pi}\sqrt{\dfrac{b}{a}}C_{23}, \end{cases} \tag{8}$$

where $C_{11}$, $C_{22}$, and $C_{23}$ are the Kalker coefficients. In the amended strip theory, the non-dimensional terms in Eq. (7) are replaced by $\xi'=c_x\xi$, $\eta'=c_y\xi$, and $\psi'=c_\varphi\psi$.

In the slip region, the longitudinal and lateral shear stresses depend on whether the strip is in full slip. For the strip including both stick and slip parts and the one in full slip, the tangential stress formulas have some differences. The detailed formulas can be found in (Kalker, 1966). However, the tangential stresses are discontinuous for the strip that consists of both stick and slip parts (Kalker, 1966), which deviates from the actual stress status. Therefore, the formulas determining the tangential stresses in strip theory for slip area are discarded in FaStrip. Instead, an elliptic traction bound is employed within the slip area with a slightly modified FASTSIM algorithm to find the stress directions.

In the FASTSIM algorithm used for stress direction, shear stresses are first calculated as

$$\bar{q}_{xf}^{n+1} = q_{xf}^{n} - \left(\frac{\upsilon_x}{L_x} - \frac{\varphi y}{L_\varphi}\right)\mathrm{d}x, \tag{9}$$

$$\bar{q}_{yf}^{n+1} = q_{yf}^{n} - \left(\frac{\upsilon_y}{L_y} + \frac{\varphi x}{L_\varphi}\right)\mathrm{d}x, \tag{10}$$

where the superscript $n$ is the discretization steps, and $L_x$, $L_y$, and $L_\varphi$ are the flexibility parameters, which can be written as $L_x$=$8a/(3C_{11}G)$, $L_y$=$8a/(3C_{22}G)$, and $L_\varphi = \pi a\sqrt{ab}/(4C_{23}G)$, respectively.

The traction bound is calculated from the parabolic contact pressure distribution and the coefficient of friction:

$$g_\mathrm{f} = \frac{2\mu N_\mathrm{f}}{\pi ab}\left[1-\left(\frac{x}{a}\right)^2-\left(\frac{y}{b}\right)^2\right]. \tag{11}$$

If the magnitude of the total shear stress $\bar{q}_\mathrm{tf} = \sqrt{\bar{q}_{xf}^2 + \bar{q}_{yf}^2}$ exceeds the traction bound, then the shear stresses are reduced accordingly:

$$q_{xf}^{n+1} = \bar{q}_{xf}^{n+1}\frac{g_\mathrm{f}}{\bar{q}_\mathrm{tf}}, \tag{12}$$

$$q_{yf}^{n+1} = \bar{q}_{yf}^{n+1}\frac{g_\mathrm{f}}{\bar{q}_\mathrm{tf}}. \tag{13}$$

The three flexibility parameters in Eqs. (9) and (10) are replaced by those for the weighted average for the point where the magnitude of the total shear stress exceeds the traction bound:

$$L_T = \frac{|\upsilon_x| L_x + |\upsilon_y| L_y + \sqrt{ab}|\upsilon_\varphi| L_\varphi}{\sqrt{\upsilon_x^2 + \upsilon_y^2 + ab\upsilon_\varphi^2}}. \tag{14}$$

Two direction coefficients in the rolling and lateral directions for each point in the slip area ($x \le -a(y)+2d(y)$) are defined as

$$r_x = \frac{q_{x\mathrm{f}}}{q_{\mathrm{tf}}}, \quad r_y = \frac{q_{y\mathrm{f}}}{q_{\mathrm{tf}}}. \tag{15}$$

The shear stress distribution in the slip area for the FaStrip is given by

$$q_x(x,y) = r_x \frac{\mu p_0}{a}\sqrt{a^2(y) - x^2}, \tag{16}$$

$$q_y(x,y) = r_y \frac{\mu p_0}{a}\sqrt{a^2(y) - x^2}. \tag{17}$$

Moreover, to improve the creep force estimation for the falling part of the creep curve in the case of pure spin for semi-axes ratios below one, the following heuristic compensation is proposed (Sichani *et al.*, 2016):

$$N_\mathrm{f} = \begin{cases} \left[1 + \left(1 - \frac{a_0}{b_0}\right)^4\right] N, & \frac{a_0}{b_0} < 1, \\ N, & \frac{a_0}{b_0} \ge 1. \end{cases} \tag{18}$$

The local creep in FaStrip is written as (Sichani *et al.*, 2016)

$$r_x(x,y) = \upsilon_x - \varphi y + c_x \frac{\mu p_0}{Ga}\left[r_x x - \kappa'\left((x - d(y)) + \sqrt{(x - d(y))^2 - (a(y) - d(y))^2}\right)\right], \tag{19}$$

$$r_y(x,y) = \upsilon_y + \varphi x + c_y \frac{\mu p_0}{Ga}\left[r_y x - \lambda'\left((x - d(y)) + \sqrt{(x - d(y))^2 - (a(y) - d(y))^2}\right)\right]. \tag{20}$$

In Eqs. (19) and (20) the elastic contribution to the local creep is included. The complete expressions of Eqs. (19) and (20) are used to estimate the local creep for the strips with stick area, while for the strips in full slip the terms involving $\kappa'$ and $\lambda'$ should be discarded.

In summary, Eqs. (1) and (2) in the stick area and Eqs. (16) and (17) in the slip area are used to evaluate the shear stresses in FaStrip, and Eqs. (19) and (20) are used to determine the local creep. These quantities are necessary for wear estimation.

### 3.3 Wear model

The wear function considering the energy dissipated in the wheel/rail contact patch with worn material, developed by the University of Sheffield (Lewis and Dwyer-Joyce, 2004; Braghin *et al.*, 2006; Lewis *et al.*, 2010) is used to evaluate wheel wear. Three wear regimes were defined in the wear function, i.e., mild, severe, and catastrophic wear corresponding to $K_1$, $K_2$, and $K_3$, respectively, in Fig. 7. The analytical expression for wear rate $K_\mathrm{w}$ (μg/(m·mm$^2$)), which expresses the weight of lost material (μg) per distance rolled (m) per contact area (mm$^2$), is given by

$$K_\mathrm{w} = \begin{cases} 5.3 I_\mathrm{w}, & I_\mathrm{w} < 10.4, \\ 55.0, & 10.4 \le I_\mathrm{w} \le 77.2, \\ 61.9 I_\mathrm{w} - 4778.7, & I_\mathrm{w} > 77.2, \end{cases} \tag{21}$$

where $I_\mathrm{w}$ (N/mm$^2$) is the local frictional power in the contact patch and can be evaluated by the means of the wear index:

$$I_\mathrm{w}(x,y) = p(x,y) \cdot \gamma(x,y), \tag{22}$$

where $p(x, y)$ and $\gamma(x, y)$ are the tractions and local creep in each point $(x, y)$ of the contact patch node, respectively.

After estimating the wear rate, the wear distribution $\delta_{p(t)}(x, y)$ at each point $(x, y)$ of the contact patch grid can be calculated as

$$\delta_{p(t)}(x,y) = \frac{K_\mathrm{w}}{\rho}\Delta x, \tag{23}$$

where $\rho$ is the density of wheel material (expressed in kg/m$^3$), and $\Delta x$ is the width of meshes of the contact patch in the rolling direction.

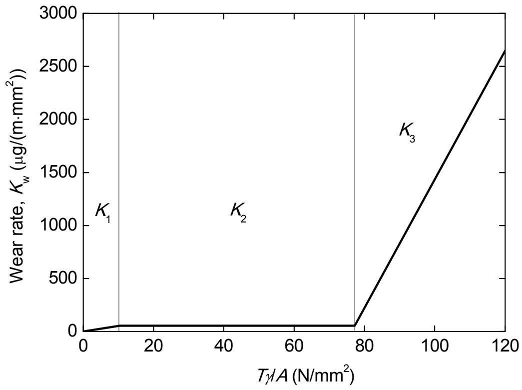


**Fig. 7 Wear rate as a function of wear index**

Then, all the wear contributions within the contact patch are summed in the longitudinal direction. The wear distribution at one cross section is achieved by

$$\delta_{p(t)}^{\mathrm{tot}}(y)=\int_{-a(y)}^{+a(y)}\delta_{p(t)}(x,y)\mathrm{d}x. \tag{24}$$

At last, the wear distribution during the dynamic simulation is summed, as

$$W_{\mathrm{d}}(y)=\frac{1}{2\pi R}\int_{T_{\mathrm{start}}}^{T_{\mathrm{end}}}\delta_{p(t)}^{\mathrm{tot}}(y)v\mathrm{d}t, \tag{25}$$

where $R$ is the nominal rolling radius, $v$ is the vehicle speed, and $T_{\mathrm{start}}$ and $T_{\mathrm{end}}$ are the start and the end times of the simulation, respectively.

## 3.4 Smoothing and updating strategy

The smoothing and updating strategy has a great influence on the accuracy of the results and the required computational effort.

### 3.4.1 Smoothing of wear distribution and wheel profile

The generation of numerical noise or the physically meaningless short spatial wavelengths in the wear distribution or in the wheel profile is inevitable. It is necessary to smooth the wear distribution and wheel profile to make the simulation more realistic and reliable. According to the wheel wear measurements, the potential wear band is defined at from −50 to 50 mm in the simulation, with a width of 100 mm. This band is divided into 601 nodes. In this study, the numerical noise and the short wavelength contributions were treated using a moving average filter, with a window width equal to 3% of the wear band. This can be written as

$$\begin{cases}W_{\mathrm{sdi}}(\mathrm{ia})=W_{\mathrm{di}}(\mathrm{ia}),\\ W_{\mathrm{sdi}}(\mathrm{ia}+1)=\sum_{\mathrm{ia}}^{\mathrm{ia}+2}W_{\mathrm{di}}(\mathrm{ia})/3,\\ W_{\mathrm{sdi}}(\mathrm{ia}+2)=\sum_{\mathrm{ia}}^{\mathrm{ia}+4}W_{\mathrm{di}}(\mathrm{ia})/5,\\ W_{\mathrm{sdi}}(j)=\sum_{j-3}^{j+3}W_{\mathrm{di}}(j)/7,\ \text{for ia}+3\le j\le \text{ib}-3,\\ W_{\mathrm{sdi}}(\mathrm{ib}-2)=\sum_{\mathrm{ib}-4}^{\mathrm{ib}}W_{\mathrm{di}}(\mathrm{ib})/5,\\ W_{\mathrm{sdi}}(\mathrm{ib}-1)=\sum_{\mathrm{ib}-2}^{\mathrm{ib}}W_{\mathrm{di}}(\mathrm{ib})/3,\\ W_{\mathrm{sdi}}(\mathrm{ib})=W_{\mathrm{di}}(\mathrm{ib}),\end{cases} \tag{26}$$

where ia and ib are the boundaries of the actual wear band, and $W_{\mathrm{di}}$ and $W_{\mathrm{sdi}}$ are the original and smoothed wear depths, respectively, of each node in the actual wear band.

Then, a spline smoothing is employed to smooth the wear distribution and the worn wheel profile before the next step. The cubic smoothing spline in MATLAB was used in this study.

### 3.4.2 Wheel profile updating

Generally, the re-profiling interval of high-speed trains is very long, reaching 200 000 km or more. It is impossible to simulate the whole distance the vehicle travelled to form the wheel wear in the wear prediction. Therefore, a scaling factor is used to amplify the wheel wear in a short simulation distance. The scaling of the distance becomes quite important to achieve results in an acceptable time. An adaptive updating strategy is used in the proposed wear model. At each simulation step, the running distance of the vehicle in the dynamic simulation ($S_{\mathrm{step}}$) is fixed as equal to the length of the virtual railway line and it is sufficiently shorter than the whole mileage. When the wheel wear calculation is done in a discrete step, the maximum wear depth ($W_{\mathrm{dmax}}$) is obtained. The value is compared with the wear depth threshold ($W_{\text{dthd}}$=0.02 mm), then the scaling factor is defined as

$$\varepsilon=\frac{W_{\text{dthd}}}{W_{\text{dmax}}}. \tag{27}$$

Thus, the running mileage at the current step is $S=\varepsilon S_{\text{step}}$ after amplification. It is necessary to set a threshold to limit the length of the running mileage in one step. A threshold of $S_{\text{thd}}$=3000 km was selected. If $S>S_{\text{thd}}$, then the scaling factor is

$$\varepsilon=\frac{S_{\text{thd}}}{S_{\text{step}}}. \tag{28}$$

The wheel wear is amplified based on the scaling factor $\varepsilon$,

$$W_{\text{dstep}}(y)=\varepsilon W_{\text{sdi}}(y). \tag{29}$$

Finally, the profile for the next step is obtained by removing the material from the current profile in the normal direction.

## 4 Model validation

The wheel profile evolution of a CRH3 high-speed train running on the Wuhan-Guangzhou high-speed railway line was monitored by the authors' research group. A total of eight measurements within a re-profiling interval were carried out. The mean worn profile and wear spreading at each measurement, as well as wear depth are shown in Fig. 8. The measurements indicate that wear spreading occurs mainly in the range from −25 mm to 25 mm relative to the nominal rolling circle of the wheel, and there is little wear generated at the wheel flange or at the root of the wheel flange. The statistics show that the wear depth clearly differed between wheels. The maximum difference was close to 0.4 mm for a running mileage of 190 000 km. There was little difference between powered and trailed wheels. That means the effect of traction forces on wear can be ignored during the simulation. It is clear from wheel profile measurements that the rate of wear occurring in the initial phase is much greater than in the next phase of service, i.e., when the wheel has run 75 000 km or more. There are two reasons for this. First, the hardness of the wheel tread increases in the initial phase, then decreases in the next phase of service. Fig. 9 shows the mean hardness measured at different stages. There is a competitive relationship between wear and hardening. The wheel tread hardness is relatively low in the initial stage, so the wear rate may be much greater than in the next phase. However, it is very difficult to take the hardening process into account during wear simulation. Second, the spread of wheel/rail contact is relatively narrow in the initial stage. The wear distribution is concentrated on a narrow contact region. This also leads to a high wear rate.

The field measurements were used to validate the wear prediction model proposed in this paper.

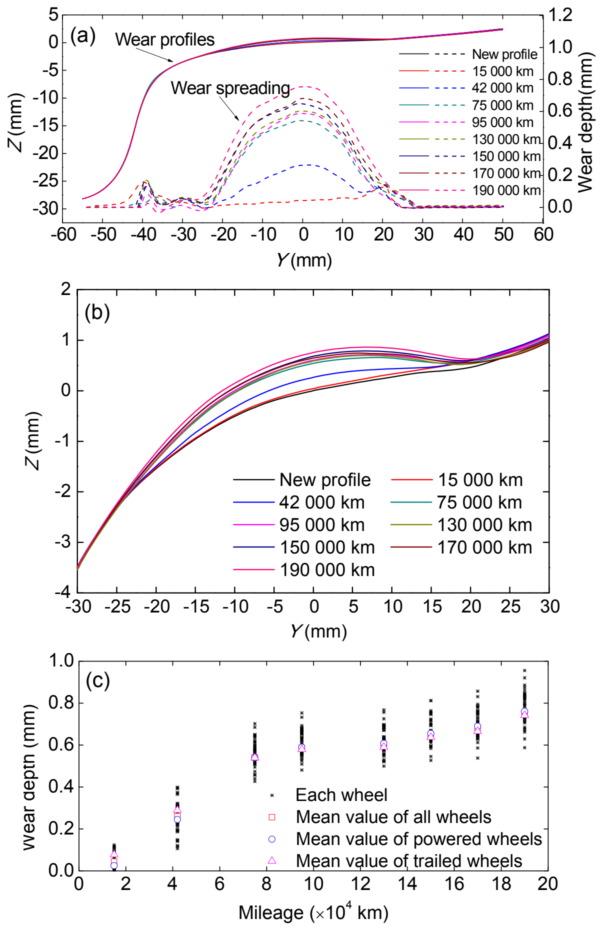


**Fig. 8 Measured wheel profiles and wear spreading with respect to mileage (Cui *et al.*, 2015) (a), the evolution of the profile in the tread zone (b), and the statistics of wear depth (c)**

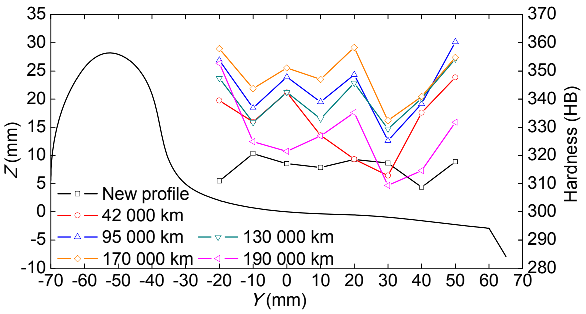


**Fig. 9 Mean hardness of the wheel tread**

To make the simulation closer to reality, a statistical approach to the Wuhan-Guangzhou line was chosen to reduce and rationalize the total simulation work. The total length of the line is 1068.8 km. The original designed speed was 350 km/h. However, the operating speed was reduced to 300 km/h from July 1st, 2011. It is impossible to perform the simulation on the real track. Therefore, an equivalent set of virtual short tracks, based on the real track of the Wuhan-Guangzhou line, was used to represent the real track.

The statistical approach to the Wuhan-Guangzhou line is given in Table 1. In accordance with the real tracks, 11 curves and the straight track were included. The tracks with curve radius $R$< 7000 m, i.e., 2500 m, 3500 m, 5500 m, and 6000 m, are located mainly near the railway station, where the train enters and/or leaves the station at braking or accelerating speed, which is variable and relatively low. To simplify the simulation, we considered the influence of accelerating and braking processes on wheel wear to be beyond the scope of this study. A relatively low speed of 200 km/h was assumed. On the curved tracks with radius $R$≥7000 m and straight track, the operating speed is generally close to the limited speed of 300 km/h. The weighted average super-elevation was used according to the percentage.

The progress of wear depth is presented in Fig. 10. The entire trend of the simulated wear depth matches well with the measured trend, but the prediction overestimates the wheel wear. The USFD wear function was carried out using a twin disc test machine. All tests to achieve the USFD wear function were performed in dry conditions without lubrication (the friction coefficient ranged from 0.45 to 0.5). The wheel specimen was cut from R8T wheel rims in the tests. The material type of the measured CHR3 wheel is ER8. The material characteristics of ER8 are similar to those of R8T. However, the actual environment at the wheel/rail interface is more complex than in the laboratory tests. Some lubrication at the wheel/rail interface, such as by water or oil, is inevitable. The wear rate will significantly decrease when water or oil is present at the wheel/rail interface (Wang W.J. *et al.*, 2016).

**Table 1 Virtual tracks based on the statistical Wuhan-Guangzhou Line**

| Radius (m) | Super-elevation (mm) | Speed (km/h) | Percentage (%) |
|---|---|---|---|
| 2500 | 150 | 200 | 0.40 |
| 3500 | 175 | 200 | 0.28 |
| 5500 | 175 | 200 | 0.96 |
| 6000 | 80 | 200 | 0.23 |
| 7000 | 148 | 300 | 0.73 |
| 8000 | 141 | 300 | 2.79 |
| 9000 | 135 | 300 | 11.84 |
| 10000 | 124 | 300 | 10.93 |
| 11000 | 114 | 300 | 5.23 |
| 12000 | 105 | 300 | 0.36 |
| 14000 | 90 | 300 | 0.09 |
| ∞ | 0 | 300 | 66.16 |

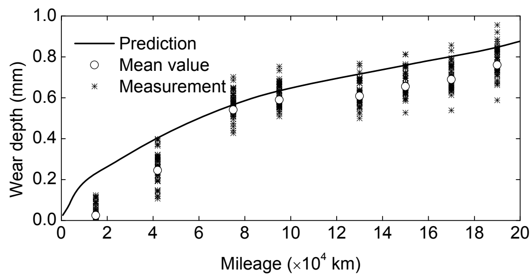


**Fig. 10 Wear depth progress with the original UFSD wear function**

The Wuhan-Guangzhou line is located mainly in Central South and South China. These areas are often damp. The wear rates used in the lab simulation may be lower than those found in actual operational conditions. Therefore, it is necessary to correct the wear rates used in the simulation. The USFD wear function comprises three parts: mild, severe, and catastrophic wear. How to correct the wear function is very important.

First of all, the wear regime should be determined. The multi-body model of the CRH3 implemented in the SIMPACK environment was used to estimate the wear index on the statistical tracks. The worn wheel profiles shown in Fig. 8 were taken as inputs for dynamic simulation. Subsequently, the global wear index of each wheel at every time step was obtained:

$$I_{\mathrm{wi}}=\left(\left|T_{xi}\upsilon_{xi}\right|+\left|T_{yi}\upsilon_{yi}\right|\right)/A_i, \tag{30}$$

where $T_{xi}$ and $T_{yi}$ are the global creep forces in the longitudinal and lateral directions, respectively, and $A_i$ is the contact area.

The maximum wear index of each worn profile for each calculation case was counted and plotted in Fig. 11. The maximum values are less than 1.0 N/mm$^2$ for all calculation cases (much less than the wear transition value of 10.4 N/mm$^2$ in the USFD wear function). This means the wheel wear is in the mild wear regime, and so only the first part of the USFD wear function was used in the simulation.

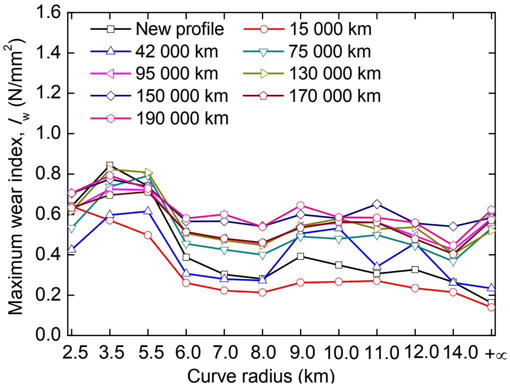


**Fig. 11 Maximum wear index in different calculation cases**

A series of factors, ranging from 0.5 to 1.0, were used to correct the wear function. The wear depth progress with different correction factors is presented in Fig. 12. The simulated results with correction factor $\zeta$=0.6 or 0.7 were very close to the measured results. Fig. 13 illustrates the simulated wheel profiles and wear spreading with $\zeta$=0.7. The predicted and measured results are in good agreement on the tread region. However, there is no wear in the flange region in the simulated results. In this paper, only the main line of the Wuhan-Guangzhou line is considered in the simulation. Generally, the curve radius is larger than 7000 m (Table 1). In addition, the turnouts and sharp curves at railway stations or the EMU depot where the high-speed trains pass at very low speed were beyond the scope of this study. Therefore, the simulation is unlikely to predict wear in the flange region. Actually, there is no wear at rail gauge corners on the main line, but the high rail of the sharp curve at the EMU depot shows obvious side wear (Fig. 14), which means that wheel flange wear occurs mainly at the EMU depot. Certainly, the turnout also contributes to flange wear.

The prediction of wheel wear with a corrected wear function is reasonable, because it is unavoidable that a number of third party materials, i.e., water and oil, will be found at the wheel/rail interface in field sites. The wear rate of wheel and rail materials decreases when water or oil is applied to the wheel/rail interface (Wang W.J. *et al.*, 2016). The wear rate is proportional to the wear index in the mild wear regime.

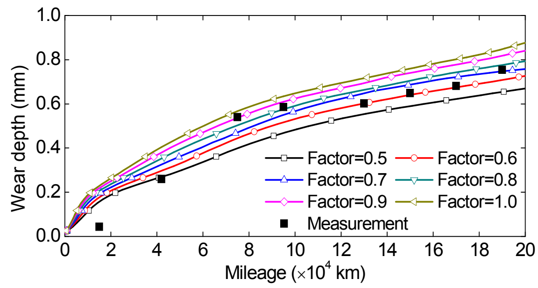


**Fig. 12 Wear depth progress with different corrected factors**

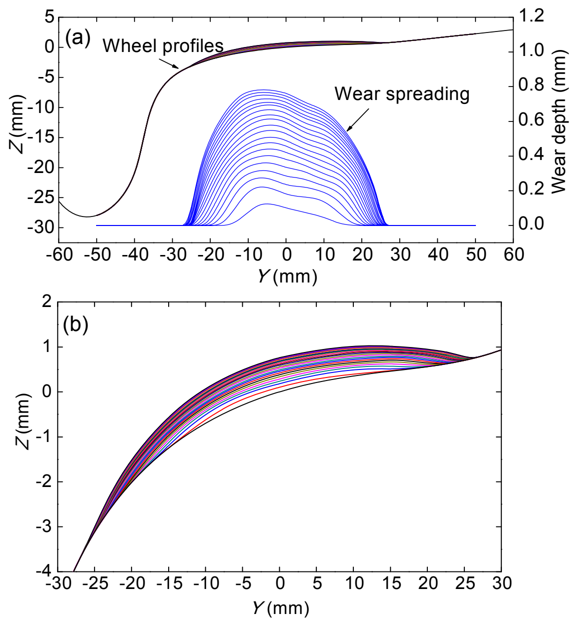


**Fig. 13 Simulated wheel profiles and wear spreading with respect to mileage (a) and the evolution of the profile in the tread zone (b)**

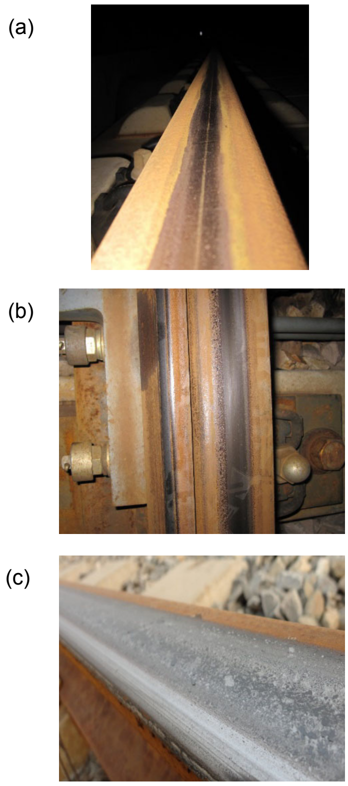


**Fig. 14 Rail wear photographs at main line (a), at turnout near railway station (b), and at EMU depot or maintenance base (c)**

According to the experimental data presented by Wang W.J. *et al*. (2016), in the mild wear regime the relationship between the wear rate and wear index can be expressed as

$$K_{\mathrm{wi}} = \alpha_{\mathrm{i}} I_{\mathrm{w}}, \tag{31}$$

where the subscript i indicates the status at the wheel/rail interface, such as dry condition or damp condition due to contamination by water, oil or other third-party materials.

Therefore, the corrected wear function can be considered as a linear combination of Eq. (31) with different weights.

The wear function is not the only factor that leads to a mismatch between the measured and simulated wear depth. Wheel wear simulation is a very complex problem. There are many factors that affect the wheel wear prediction results, such as normal and tangential contact solutions, dynamic simulations, wear functions, smoothing and updating of profiles, curve radius distributions, rail profiles, track irregularities, and the friction coefficient at the wheel/rail interface. Moreover, it is difficult to take into account the hardening process and plastic deformation of wheel material in the simulation. These factors could cause some differences between the results from simulation and measurement. The wear function, friction coefficient, and the modelling of the wheel/rail contact are the key factors that affect the accuracy of wheel wear prediction. Using a more accurate contact model, like CONTACT developed by Kalker (1990) or the finite element model developed by Li *et al.* (2008a; 2008b) and Zhao and Li (2011), may lead to more accurate results. But the computational cost could be inestimable, because it needs to simulate the running distance of more than 200 000 km. Therefore, using a simplified model to solve the contact problem in wheel wear simulation may be a good choice as a compromise between calculation efficiency and accuracy (Tao *et al*., 2016). The wear model developed in this paper is very efficient. The computational time is about 50 h to evaluate the wheel wear for a running mileage of 200 000 km. The time depends greatly on the wear depth threshold and the running mileage threshold in a single step.

Modifying the wear function is a simple way to match the predicted and measured results. This validation is very important for further research, such as the optimization of the wheel re-profiling interval and estimation of a wheel's service life.

## 5 Conclusions

A comprehensive wear model for the prediction of the evolution of high-speed train wheel profiles due to wear is presented in this paper. The specially developed model consists of four modules: a multi-body model implemented with the commercial multi-body software SIMPACK to evaluate the dynamic response of the vehicle and track; a local contact model with Hertzian theory and a novel and versatile method, named FaStrip, to calculate the normal and tangential forces, respectively; a wear model proposed by the University of Sheffield (known as the USFD wear function) to estimate the amount of removed material and its distribution along the wheel profile; and a smoothing and updating strategy.

Simulation of the wheel wear of the CRH3 high-speed train in service on the Wuhan-Guangzhou high-speed railway line was carried out. A virtual railway line based on the statistics of the line was used to represent the entire real track. The model was validated using wheel wear data of the CRH3 high-speed train operating on the same line, monitored by the authors' research group.

The outputs of the wear model with the corrected USFD wear function were very consistent with field measurements, both for wear depth and wear spreading. However, some aspects still need improvement. Firstly, the flexibility of the track is ignored in the current model. Some previous research indicated that track flexibility should not be neglected, as it has a significant influence on wheel/rail contact behavior (Jin *et al*., 2002; Zhai *et al*., 2009; Di Gialleonardo *et al*., 2012), such as wheel/rail contact positions, creepages, spin, and creep forces. These quantities are closely related to wear estimation. Secondly, the versatile contact model FaStrip was used in post-processing rather than online dynamic solutions, and Kalker (1982)'s simplified theory FASTSIM was used in dynamic simulation. This may cause discrepancies, because the contact stiffness at the wheel/rail interface is dependent on the contact model in use. Thirdly, a new rail profile rather than worn profiles measured on the real tracks was adopted in the simulation, which may have affected the predictions, especially for wear spreading. Finally, measurement of the friction coefficient is necessary. Consideration of the dispersion of possible values of the friction coefficient based on the field measurements will make the simulation more realistic. In future, a more complete wear model should be considered, which includes a coupling vehicle/track model taking track flexibility into account, and a versatile contact model implemented with an online solution.

## References


Archard, J.F., 1953. Contact and rubbing of flat surfaces. *Journal of Applied Physics*, **24**:981-988. http://dx.doi.org/10.1063/1.1721448

Auciello, J., Ignesti, M., Malvezzi, M., *et al*., 2012. Development and validation of a wear model for the analysis of the wheel profile evolution in railway vehicles. *Vehicle System Dynamics*, **50**(11):1707-1734. http://dx.doi.org/10.1080/00423114.2012.695021

Ayasse, J.B., Chollet, H., 2005. Determination of the wheel rail contact patch in semi-Hertzian conditions. *Vehicle System Dynamics*, **43**(3):161-172. http://dx.doi.org/10.1080/00423110412331327193

Braghin, F., Lewis, R., Dwyer-Joyce, R.S., *et al*., 2006. A mathematical model to predict railway wheel profile evolution due to wear. *Wear*, **261**(11-12):1253-1264. http://dx.doi.org/10.1016/j.wear.2006.03.025

Cui, D.B., Wang, H.Y., Li, L., *et al*., 2015. Optimal design of wheel profiles for high-speed trains. *Proceedings of the Institution of Mechanical Engineers, Part F: Journal of Rail and Rapid Transit*, **229**(3):248-261. http://dx.doi.org/10.1177/0954409713509979

Di Gialleonardo, E., Braghin, F., Bruni, S., 2012. The influence of track modelling options on the simulation of rail vehicle dynamics. *Journal of Sound and Vibration*, **331**(19): 4246-4258. http://dx.doi.org/10.1016/j.jsv.2012.04.024

Ding, J., Sun, S., Qi, Z., *et al*., 2013. Wheel wear prediction of railway freight car based on wheel/rail creep mechanism. *Tribology*, **33**(3):236-244 (in Chinese).

Ding, J., Li, F., Huang, Y., *et al*., 2014. Application of the semi-Hertzian method to the prediction of wheel wear in heavy haul freight car. *Wear*, **314**(1-2):104-110. http://dx.doi.org/10.1016/j.wear.2013.11.052

Enblom, R., Berg, M., 2005. Simulation of railway wheel profile development due to wear–influence of disc braking and contact environment. *Wear*, **258**(7-8):1055-1063. http://dx.doi.org/10.1016/j.wear.2004.03.055

Han, P., Zhang, W., 2015. A new binary wheel wear prediction model based on statistical method and the demonstration. *Wear*, **324-325**:90-99. http://dx.doi.org/10.1016/j.wear.2014.11.022

Ignesti, M., Marini, L., Meli, E., *et al*., 2012a. Development of a model for the prediction of wheel and rail wear in the railway field. *Journal of Computational and Nonlinear Dynamics*, **7**(4):041004. http://dx.doi.org/10.1115/1.4006732

Ignesti, M., Malvezzi, M., Marini, L., *et al*., 2012b. Development of a wear model for the prediction of wheel and rail profile evolution in railway systems. *Wear*, **284-285**: 1-17. http://dx.doi.org/10.1016/j.wear.2012.01.020

Ignesti, M., Innocenti, A., Marini, L., *et al*., 2013. Development of a model for the simultaneous analysis of wheel and rail wear in railway systems. *Multibody System Dynamics*, **31**(2):191-240. http://dx.doi.org/10.1007/s11044-013-9360-0

Innocenti, A., Marini, L., Meli, E., *et al*., 2014. Development of a wear model for the analysis of complex railway networks. *Wear*, **309**(1-2):174-191. http://dx.doi.org/10.1016/j.wear.2013.11.010

Jendel, T., 2002. Prediction of wheel profile wear–comparisons with field measurements. *Wear*, **253**(1-2): 89-99. http://dx.doi.org/10.1016/S0043-1648(02)00087-X

Jin, X.S., Wu, P.B., Wen, Z.F., 2002. Effects of structure elastic deformations of wheelset and track on creep forces and wheel/rail rolling contact. *Wear*, **253**(1-2):247-256. http://dx.doi.org/10.1016/S0043-1648(02)00108-4

Kalker, J.J., 1966. A Strip Theory for Rolling with Slip and Spin. Internal Report 327, Department of Mechanical Engineering, Delft University of Technology, the Netherlands.

Kalker, J.J., 1967. On the Rolling Contact of Two Elastic Bodies in the Presence of Dry Friction. PhD Thesis, Delft University of Technology, the Netherlands.

Kalker, J.J., 1982. A fast algorithm for the simplified theory of rolling contact. *Vehicle System Dynamics*, **11**(1):1-13. http://dx.doi.org/10.1080/00423118208968684

Kalker, J.J., 1990. Three-dimensional Elastic Bodies in Rolling Contact. Kluwer Academic Publishers, Dordrecht, the Netherlands.

Lewis, R., Dwyer-Joyce, R., 2004. Wear mechanisms and transitions in railway wheel steels. *Proceedings of the Institution of Mechanical Engineers, Part J: Journal Engineering Tribology*, **218**(6):467-478. http://dx.doi.org/10.1243/1350650042794815

Lewis, R., Dwyer-Joyce, R., Olofsson, U., *et al*., 2010. Mapping railway wheel material wear mechanisms and transitions. *Proceedings of the Institution of Mechanical Engineers, Part F: Journal of Rail and Rapid Transit*, **224**(3): 125-137. http://dx.doi.org/10.1243/09544097JRRT328

Li, X., Jin, X.S., Wen, Z.F., *et al*., 2011. A new integrated model to predict wheel profile evolution due to wear. *Wear*, **271**(1-2):227-237. http://dx.doi.org/10.1016/j.wear.2010.10.043

Li, Z., Zhao, X., Dollevoet, R., *et al*., 2008a. Differential wear and plastic deformation as causes of squat at track local stiffness change combined with other track short defects. *Vehicle System Dynamics*, **46**(sup1):237-246. http://dx.doi.org/10.1080/00423110801935855

Li, Z., Zhao, X., Esveld, C., *et al*., 2008b. An investigation into the causes of squats—correlation analysis and numerical modeling. *Wear*, **265**:1349-1355. http://dx.doi.org/10.1016/j.wear.2008.02.037

Sichani, M.Sh., Enblom, R., Berg, M., 2016. An alternative to FASTSIM for tangential solution of the wheel/rail contact. *Vehicle System Dynamics*, **54**(6):748-764. http://dx.doi.org/10.1080/00423114.2016.1156135

Tao, G.Q., Wen, Z.F., Zhao, X., *et al*., 2016. Effects of wheel-rail contact modelling on wheel wear simulation. *Wear*, **366-367**:146-156. http://dx.doi.org/10.1016/j.wear.2016.05.010

Wang, J.B., Song, C.Y., Wu, P.B., *et al*., 2016. Wheel re-profiling interval optimization based on dynamic behavior evolution for high-speed trains. *Wear*, **366-367**: 316-324. http://dx.doi.org/10.1016/j.wear.2016.06.016

Wang, W.J., Lewis, R., Yang, B., *et al*., 2016. Wear and damage transitions of wheel and rail materials under various contact conditions. *Wear*, **362-363**:146-152. http://dx.doi.org/10.1016/j.wear.2016.05.021

Zhai, W.M., Wang, K.Y., Cai, C.B., 2009. Fundamentals of vehicle-track coupled dynamics. *Vehicle System Dynamics*, **47**(11):1349-1376. http://dx.doi.org/10.1080/00423110802621561

Zhao, X., Li, Z., 2011. The solution of frictional wheel/rail rolling contact with a 3D transient finite element model: validation and error analysis. *Wear*, **271**(1-2):444-452. http://dx.doi.org/10.1016/j.wear.2010.10.007

Zobory, I., 1997. Prediction of wheel/rail profile wear. *Vehicle System Dynamics*, **28**(2-3):221-259. http://dx.doi.org/10.1080/00423119708969355

## 中文概要

**题　目：**高速列车车轮磨耗预测模型的发展及验证

**目　的：**高速列车车轮磨耗过程非常复杂，涉及因素较多。本文旨在发展及验证一个高速列车车轮磨耗预测模型，对高速铁路轮轨型面设计、车辆悬挂参数设计、车轮镟修计划的制订及降低运营维护成本等具有非常重要的意义。

**创新点：**1. 建立一个包含车辆轨道动力学仿真、轮轨局部接触求解、车轮磨耗计算和型面平滑与更新策略的高速列车车轮磨耗预测模型；2. 利用跟踪测试的高速列车车轮磨耗结果对预测模型进行验证；3. 修正 USFD 磨耗函数，使得预测结果与实测结果更为吻合。

**方　法：**1. 在 SIMPACK 多体动力学软件中建立 CRH3 型动车组拖车的动力学模型，对武广高铁的实际线路进行统计，采用统计的虚拟线路代替实际线路；2. 利用 FaStrip 进行轮轨局部接触求解；3. 采用修正后的 USFD 磨耗函数进行车轮磨耗计算；4. 利用现场实测数据验证模型的可靠性。

**结　论：**轮轨界面状态对车轮磨耗具有较大的影响；直接采用已有的磨耗模型进行车轮磨耗预测可能会导致一定的偏差，需要对其进行适当的修正才能获得较好的预测结果。

**关键词：**高速列车；车轮型面；轮轨接触；车轮磨耗预测